Frequency Stability Enhancement of the Grid-Following and Grid-Forming Control with Emulated Inertia and Damping

Yang, Fan; Yu, Haoyuan; Wang, Lu; Bauer, Pavol; Qin, Zian

DOI
10.1109/PEDG62294.2025.11060217

Publication date
2025

Document Version
Final published version

Published in
PEDG 2025 - 2025 IEEE 16th International Symposium on Power Electronics for Distributed Generation Systems

Citation (APA)
Yang, F., Yu, H., Wang, L., Bauer, P., & Qin, Z. (2025). Frequency Stability Enhancement of the Grid-Following and Grid-Forming Control with Emulated Inertia and Damping. In *PEDG 2025 - 2025 IEEE 16th International Symposium on Power Electronics for Distributed Generation Systems* (pp. 62-67). (PEDG 2025 - 2025 IEEE 16th International Symposium on Power Electronics for Distributed Generation Systems). IEEE. https://doi.org/10.1109/PEDG62294.2025.11060217

2025 IEEE 16th International Symposium on Power Electronics for Distributed Generation Systems (PEDG) | 979-8-3315-8549-5/25/$31.00 ©2025 IEEE | DOI: 10.1109/PEDG62294.2025.11060217

Frequency Stability Enhancement of the Grid-following and Grid-forming Control with Emulated Inertia and Damping

Fan Yang, Haoyuan Yu, Lu Wang, Pavol Bauer, Zian Qin
Department of Electrical Sustainable Energy, Delft University of Technology
Mekelweg 4, 2628CD, Delft, The Netherlands
Emails: {F.Y.Yang-1, H.Yu-6, L.Wang-11, P.Bauer, Z.Qin-2}@tudelft.nl

***Abstract*—Grid-following control (GFL) has been widely implemented as the dominant control method for inverter-based resources (IBR). However, because GFL cannot provide sufficient inertia for frequency regulation, grid-forming control (GFM) is proposed as an alternative solution. However, the impact of grid dynamics characteristics on GFL and GFM control is rarely discussed. Therefore, this paper systematically derives and compares the frequency response of GFL and GFM control, considering the grid dynamics that are emulated by a synchronous generator. The impact of the inertia of GFM is investigated by pole-zero maps. Simulations are given to verify the effectiveness**

***Index Terms*—Emulated inertia, frequency response, grid-following control, grid-forming control, frequency stability**

I. Introduction

The widespread installation of renewable sources has led to an energy transition from a Synchronous Generator (SG) dominated grid to an Inverter-based resources (IBR) [1]. Unlike a conventional power grid composed of SGs, the high penetration of IBR reduces the whole system's inertia.

High inertia decreases the value of RoCoF and supports the frequency nadir, which leaves more space for the hierarchy frequency regulation. Following the inertia response, Primary Frequency Regulation (PFR) and Secondary Frequency Regulation respond to the system, compensating for the power [2], [3] caused by the disturbance and re-stabilizing the frequency to the nominal value [4], [5].

Much work has been done to configure the grid-connected inverters' control mode to provide the "emulated inertia" [6]. Paper [7], [8]qualitatively analyzes the frequency response of different generation units, which lacks an analytical model and quantitative results. Paper [9], [10] claims synthetic inertia control with a modified swing equation. However, the grid model is simplified as a voltage source. To mitigate these research gaps, this paper analytically models the converter-SG system and compares the GFL, GFM, and SG frequency response. The grid is modeled as an SG with a turbine, governor, and exciter dynamics, providing a whole system map.The contributions of this paper are as follows:

1) The function of inertia and damping in the frequency support is revealed and analyzed.

2) The dynamics of a VSM-controlled GFM converter and an SG are modeled analytically by transfer functions and verified by simulations.

3) The impact of VSM parameters tuning is revealed with the derived model.

The rest of this paper is organized as follows: Section II presents the SG, GFM, and GFL control models. Section III derives the system's transfer function and reveals the parameters' impact. Section IV shows the simulation results and discusses the impact of the parameter settings. Finally, the conclusions are drawn in Section V. The parameters of the models are given in the Appendix.

II. Modelling of System

A. SG-converter Connected Model

A synchronous generator model connected with a power converter is used as the model for the frequency response, shown in Fig.1. The power converter with GFL or GFM modes and connected to an SG with a grid impedance L_g. A step load disturbance R_l is set to mimic the load disturbance. R_f and L_f are the converter resistor and inductor filter, respectively.

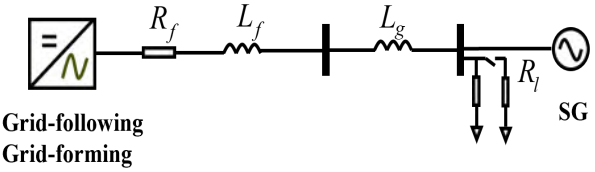

Fig. 1: The simplified structure of the system.

The grid impedance L_g is given by the Short Circuit Ratio (SCR) value, which is calculated as:

$$L_g = \frac{3E_g^2}{\omega_n S_{nCON} SCR} \tag{1}$$

E_g is the grid voltage, ω_n is the grid frequency, S_{nCON} is the converter apparent rated power. To better illustrate the system's model, the power converter's control structure is given in Fig.2, which provides a direct intuition of the grid-following control and the grid-forming control. As shown in Fig.2, for a PLL is implemented to track the grid frequency. The principle of a PLL is to control the Q-axis voltage to 0 through a PI controller [11]. By properly tuning

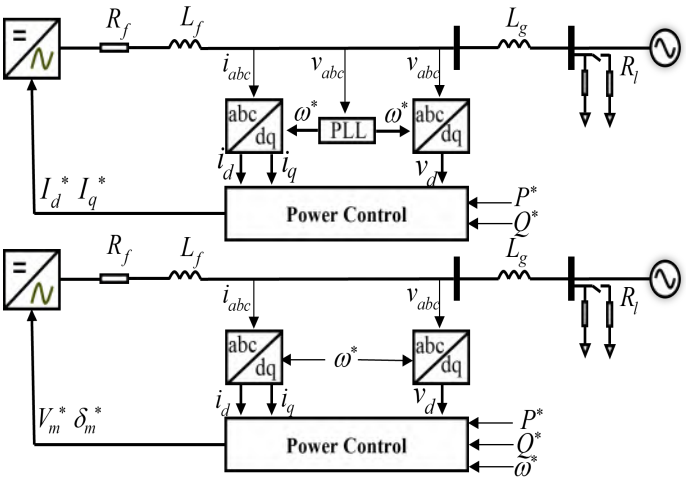

Fig. 2: Power control of GFL and GFM.

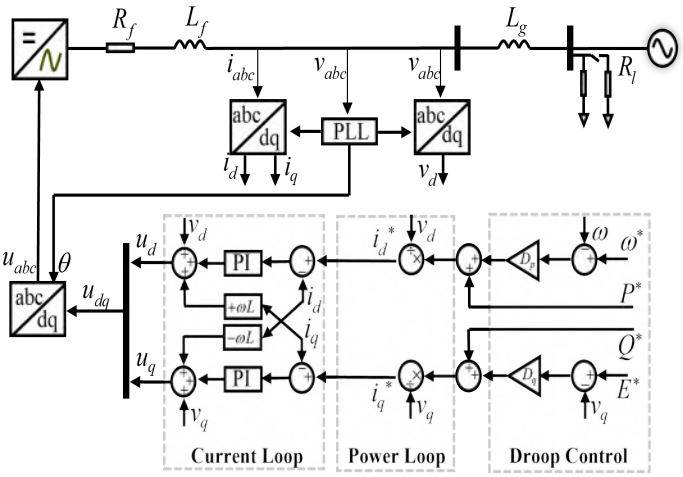

Fig. 3: Control structure of a GFL control with power droop.

the bandwidth of the PLL, the converter tracks the frequency of the Point of Common Coupling (PCC) perfectly. Based on the frequency reference, Clarke-Park transformation converts the abc frame to dq frame, finally giving the current reference signal I_d^*, I_q^*. In contrast to GFL control, the reference frequency of GFM control is produced by the outer control loop, referred to as a Power-synchronization loop [12]. The voltage reference signal V_m^* and angle reference signal δ_m^* are produced based on the reference frequency. To draw a short conclusion, GFL control is the current control mode, while GFM is equivalent to a controlled voltage source. The details of GFL control and GFM control are introduced in the following content.

B. Grid-following Control

Fig.3 depicts the control structure of a GFL control with an added outer frequency-power droop. A power droop loop is set as the outer loop for the GFL control to provide the inertia power, which provides the frequency response.

The outer loop is the power droop, which calculates the reference active power P and reactive power Q. The power loop calculates the current reference signals i_d^*, i_q^* for the current loop. With feed-forward compensation, the current loop is decoupled. Finally, the voltage reference signals u_d, u_q are generated. v_{abc}, i_{abc} are the measured values of the voltage and current of PCC, respectively. ω^*, P^*, Q^*, E^* are the reference frequency, active power, reactive power and voltage. Eq. (2) gives the damping power provided by the grid-following converter under the frequency variation.

$$P = P^* + D_p(\omega^* - \omega) \tag{2}$$

C. Grid-forming Control

Similar to the GFL control structure, GFM control also has a current loop, a voltage loop, and an outer frequency-power loop shown in Fig.4. Eq. (3) gives the relationship between frequency ω and active power, referred to as the swing equation. P^* and P_m are the reference and measured converter output power. M is the inertia constant, and D_p is the damping factor. With the reference phase angle θ obtained from the VSM loop, the Clarke-Parke transformation converts the coordinate to a stationary reference frame, which conducts the voltage and current control accordingly. Eq. (3) expresses the inertia power provided by the Grid-forming converter under the frequency variation.

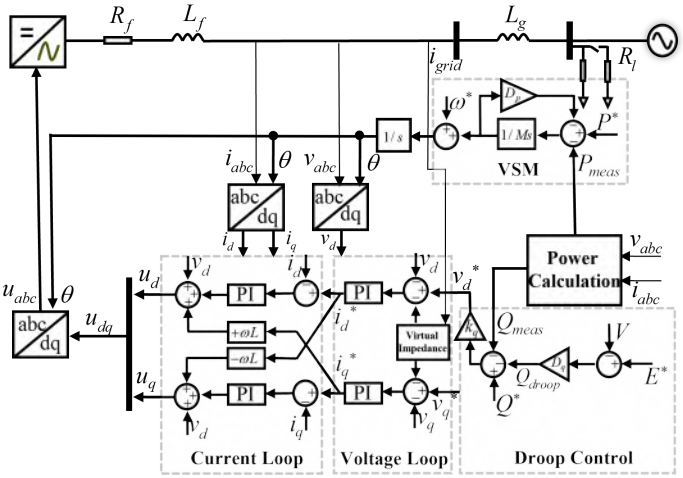

Fig. 4: Control structure of a Grid-forming control in VSM mode.

$$P^* - P = M\dot{\omega} + D_p(\omega^* - \omega) \tag{3}$$

As the control mode of GFM is voltage control, the inner loop, such as the Voltage Loop and Current Loop, can be omitted if desired. The voltage reference signals u_d and u_q are re-converted to three phase coordinates directly, which produces PWM modulation signals for the Voltage Source Converter (VSC).

III. Block Diagram and System dynamics

A. SG-Converter Model

The system transfer function is derived based on the model introduced in Section II. Fig.5 gives the block diagram of the SG-converter model that is shown in Fig.1. Only the active power loop is considered to simplify the system, which reflects the frequency variation. The grid impedance is set as purely inductive. Based on these assumptions, the active power can be controlled by controlling θ directly, which is the basis of the droop control strategies of load sharing [13].

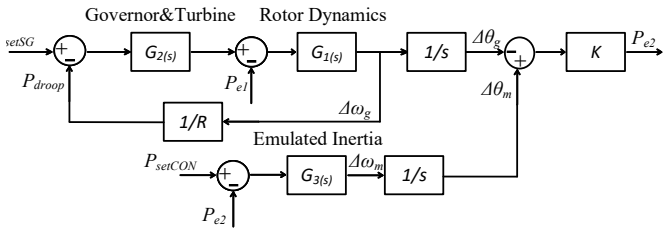

Fig. 5: The P-θ characteristics of the whole system.

The model is divided into two parts: the SG model and the converter model. The definitions of the variables are illustrated below:P_{setSG} is the nominal power of the SG, and P_{droop} is the droop compensation power of the generator droop control. P_{setCON} is the nominal power of the converter. R is the droop coefficient of the governor control. Eq. (4) defines the active power sharing between two sources. P_{e1}, P_{e2} are the active power the SG and converter provide, which sums up the total load power.

$$P_{e1} + P_{e2} = P_L \quad P_{e2} = \frac{E_g^2}{X_L}(\Delta\theta_m - \Delta\theta_g) \tag{4}$$

Eq. (5) is written by substituting the phase angle θ to converter frequency ω_m and grid frequency ω_g.

$$P_{e2} = \frac{E_g^2}{X_L}(\frac{\Delta\omega_m}{s} - \frac{\Delta\omega_g}{s}) \tag{5}$$

$G_1(s), G_2(s), G_3(s)$ are the transfer functions that describe the dynamics of the SG inertia, Governor&Turbine dynamics, and the converter frequency dynamics. To better evaluate the impact of the emulated inertia of the converters, the concept of the frequency of center of inertia (CoI) [14] is introduced:

$$\omega_{sys} = \frac{\sum_{i=1}^{N} H_i\omega_i}{\sum_{i=1}^{N} H_i} = \frac{H_{SG}\omega_g + H_{Conv}\omega_m}{H_{SG} + H_{Conv}} \tag{6}$$

The CoI frequency is calculated using the grid-connected source frequency ω_g, ω_m and the synchronous generator's inertia time constant H and M of the converter.

B. System Transfer Functions

The block diagram of the SG and GFL/GFM converter gives the RoCoF frequency dynamics under a load-step scenario, which is shown in Fig.6.

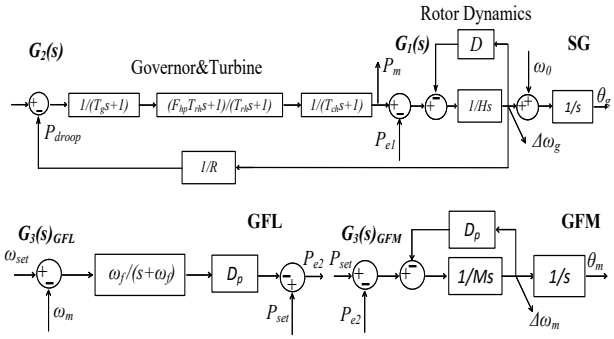

Fig. 6: Block diagram of the active power loop.

The swing equations of the SG , GFL, and GFM converters are derived as below:

$$G_1(s) = \frac{1}{Hs + D} \tag{7}$$

$$G_2(s) = \frac{F_{hp}T_{rh}s + 1}{(T_g s + 1)(T_{rh}s + 1)(T_{ch}s + 1)} \tag{8}$$

$G_1(s)$ is the SG rotor dynamics. $G_2(s)$ is the dynamics of the governor and turbine. T_g, T_{rh}, T_{ch} are the governor time constant, the re-heater's turbine time constant, and the steam inlet's turbine time constant. The swing equation of the SG is calculated as:

$$\Delta\omega_g = \frac{RG_1(s)G_2(s)}{R + G_1(s)G_2(s)}\Delta P_{set1} - \frac{RG_1(s)}{R + G_1(s)G_2(s)}\Delta P_{e1} \tag{9}$$

P_{set1} is set as a constant value, with the expression of ΔP_{e1}, the transfer function of grid frequency is obtained. As P_{e1} is calculated by eq. (4), the swing equations of GFL and GFM are referred to in Fig 6. The swing equation of GFL contains the dynamic of a PLL and a damping (droop) compensation [15]. ζ_i, ω_{pll_i} are the damping and bandwidth.

$$\omega_{PLL} = \frac{2\zeta_i\omega_{pll_i}s + \omega_{pll_i}^2}{s^2 + 2\zeta_i\omega_{pll_i}s + \omega_{pll_i}^2}\omega_m \quad \omega_{PLL} = G_{PLL}\omega_m \tag{10}$$

Based on eq. (2) and eq. (10), the damping of PLL is set as a relatively high value. G_{PLL} is rewritten as a low pass filter, and the swing equation of GFL is written as:

$$G_{3GFL}(s) = \frac{1}{D_p G_{PLL}} \quad G_{PLL} = \frac{\omega_f}{s + \omega_f} \tag{11}$$

Similar to the swing equation of GFL. The swing equation of GFM control is derived from Equation (3), which is given as:

$$G_{3GFM}(s) = \frac{1}{Ms + D_p} \tag{12}$$

Taking eq. (7),(8),(9),(10),(11),(12) into eq. (5), the inertia power P_{e2} is calculated as:

$$P_{e2}(s) = \frac{KRG_1}{KG_1G_2G_3 + KR_d(G_1+G_3) + s(G_1G_2+R)} P_L \tag{13}$$

$K = \frac{E_g^2}{X_L}$ is a constant given by the grid parameters. To be noticed, both of the $P_{e2GFL}(s)$ and $P_{e2GFM}(s)$ can be calculated by eq. (13), with the change of $G_3(s)$ to $G_{3GFL}(s)$ and $G_{3GFM}(s)$ respectively. Rewrite eq. (9) as:

$$\omega_g(s) = \frac{R_dG_1(s)(P_L(s) - P_{e2}(s))}{R_d + G_1(s)G_2(s)} \tag{14}$$

Take eq.(13) into eq.(14), the transfer function of the SG (grid) frequency is obtained. The transfer function of RoCoF is also obtained by calculating the derivative of eq.(14). Similarly, the converter frequency of the GFL converter ω_{GFL} and GFM converter ω_{GFM} is obtained as:

$$\omega_{mGFL} = P_{e2GFL}(s)G_{3GFL}(s) \tag{15}$$

$$\omega_{mGFM} = P_{e2GFM}(s)G_{3GFM}(s) \tag{16}$$

Reconsidering the inertia power P_{e2}, which is given in eq. (13), the values of damping (droop) factor D_p can be certified. Applying the Laplace Final Value Theorem to get the steady state power provided by the converter (The load disturbance is set as a step signal):

$$P_{e2s} = \lim_{t\to\infty} P_{e2}(t) = \lim_{s\to 0} sP_{e2}(s)\frac{1}{s} \tag{17}$$

Similarly, the steady-state value is obtained as :

$$\omega_{syss} = \lim_{t\to\infty} \frac{\omega_m(t)M + \omega_g(t)H}{M+H} = \lim_{s\to 0} \frac{s\omega_m(s)M + s\omega_g(s)H}{M+H} \tag{18}$$

The analytical expressions of the steady state converter power P_{e2s} and frequency drop $\Delta\omega_{syss}$ are given as follows:

$$P_{e2s} = \frac{D_pR}{DR + D_pR + 1} \quad \Delta\omega_{syss} = \frac{R}{DR_d + D_pR_d + 1} \tag{19}$$

From eq. (19), it can be concluded that the steady state power is only determined by the converter damping coefficient D_p, rotor damping coefficient D, and governor droop factor R. For this SG-converter model, the maximum value of D_p is determined by the nominal power of the converter as it is the only value that can be tuned for the converter. Adding D_p to the system increases the converter output power, which gives less frequency variation.

C. Parameters Settings

The pole-zero map of GFL and GFM are plotted based on eq. (13) to study the impact of GFL and GFM parameter settings. Inertia time constant M, and damping(droop) coefficient D_p are investigated, respectively. The pole-zero map of the inertia time constant M based on transfer function eq. (13) is plotted as Fig.7. The emulated inertia provided by GFM control can increase the system's inertia, but a high inertia time constant M oscillates the system during the transient.

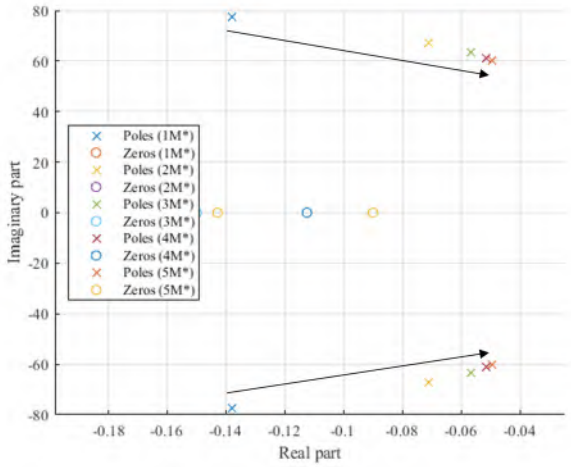

Fig. 7: Pole-zero map of inertia constant M.

The value of M varies from M^* to $5M^*$, which gives inertia from the rated value to 5 times. It can be inspected that with the increase of inertia constant M, the dominant poles move towards the imaginary axis from the negative direction. The converter output power becomes more oscillatory or even unstable, which may damage the converter due to the limited overcurrent capability.

One solution for maintaining the system stability while providing the required inertia is to increase the damping coefficient value D_p. The pole-zero map of $D_p = 4D_{P*}$ is plotted as Fig.8.

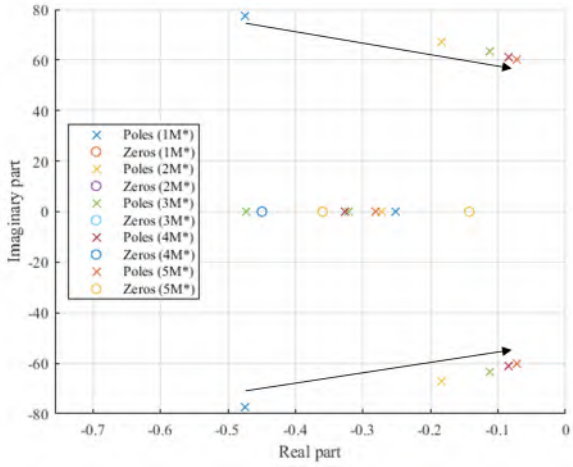

Fig. 8: Pole-zero map of $D_p = 4D_p^*$.

Comparing the real axis of Fig.7 and Fig.8, it can be concluded that the increase of D_p moves the dominant poles far from the imaginary axis, which gives more stability margin under a high inertia constant value M.

IV. Simulation and Verification

A. Model Verification

GFL and GFM control simulations are built based on the control structure proposed in Fig.3 and Fig.4. The transfer function of converter power P_{e2} is compared with the simulation results obtained from PLECS. Fig.9 shows the simulation results in PLECS and transfer functions OF Matlab.

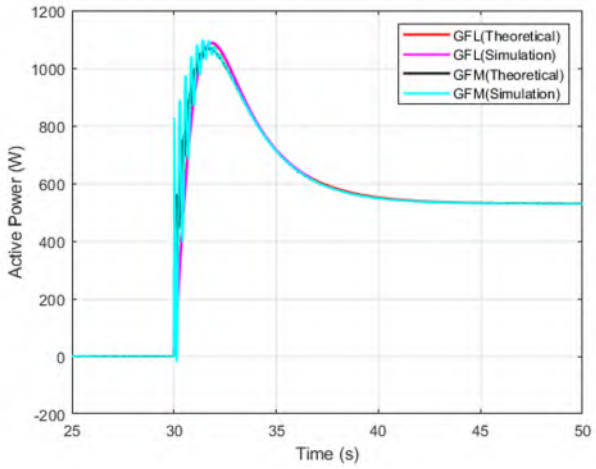

Fig. 9: Comparison of Matlab transfer function and PLECS simulation.

The converter's nominal power is set at 3kW. A load step occurs at 30s, which simulates the load disturbance. The converter responds to the system immediately by providing power. After a short transient of about 5s, the converter outputs the steady-state power, which is determined by the load-sharing settings with the SG. From the figure, it can be concluded that the transfer functions listed perfectly represent the simulation models and can be used for further analysis.

B. Frequency Response

The effects of damping coefficient D_p and inertia constant M are analyzed. To verify the conclusion, the frequency response of GFL and GFM after a load step at 30s is plotted, shown as Fig.10.

The figure shows that GFL and GFM control have the same steady state frequency, 49.80Hz, which verifies that the GFL control can also support the grid frequency. Compared to the steady state frequency of the SG without a converter connected, 49.76Hz, it can be concluded that the injection of the converters' active power helps increase the frequency by sharing the load. Also, because of the active power provided by the converters, the system has a much higher frequency nadir, which enhances the frequency stability. Another interesting phenomenon is that compared to GFL, GFM provides the emulated inertia, which increases the system inertia. Hence, the GFM control gives a higher frequency nadir value. Because of the same damping factor D_p value of GFL and GFM, the final frequency of GFL and GFM is the same value.

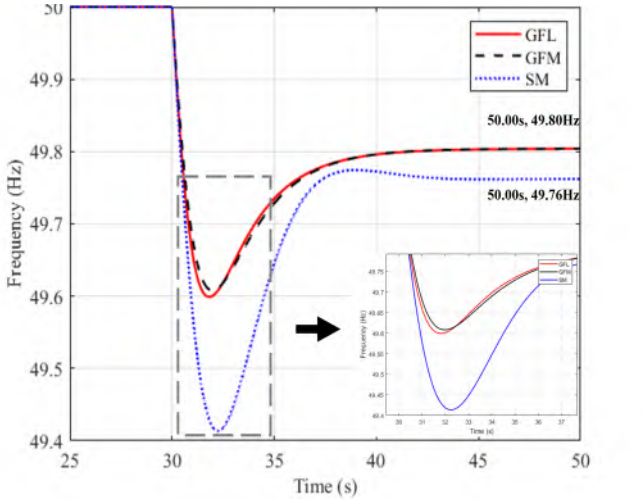

Fig. 10: Frequency response of GFL, GFM, and SG.

Another function of the emulated inertia is to limit the maximum value of RoCoF. Compared to GFL, the emulated inertia adds system inertia, which limits RoCoF. As the largest value of RoCoF occurs at the beginning of the load change, Fig.11 is plotted to show the maximum value of the RoCoF.

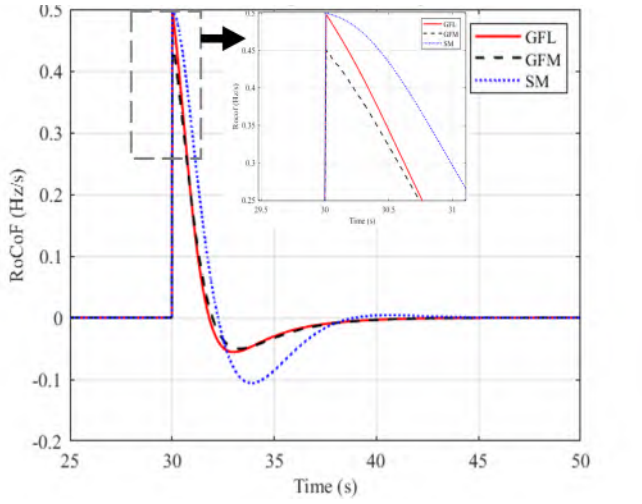

Fig. 11: Maximum value of RoCoF of GFL, GFM, and SG.

Without the emulated inertia provided by the GFM control, GFL and SG have the same maximum RoCoF value, 0.5Hz/s. In comparison, the GFM control decreases the maximum RoCoF to 0.45Hz/s, giving more tolerance for a RoCoF-sensitive system. After the load disturbance, as GFL control also provides power to the system, an SG with a converter, either GFL or GFM connected, can decrease the RoCoF of the system. The maximum value of the RoCoF is limited by the SG inertia and emulated inertia from GFM control.

V. Results and conclusions

This paper compares the frequency response of a single SG and an SG connected with a converter in GFL or GFM mode. The similarities and differences in the control structure of the GFL and GFM control loops are discussed. The transfer function of the SG-converter-connected model is derived based on the swing equation of the GFL and GFM control and the SG. The CoI frequency, inertia, and converter output power analytical expressions are given and used for the load-step analysis. Compared to GFL, GFM control provides emulated inertia to the system, which increases the system inertia and limits the maximum value of RoCoF. By setting the value of the damping coefficient D_p, the steady state frequency drop and the converter output power are certified. Besides, the higher value of D_p can also suppress the oscillation brought by the immense inertia time constant value of H. The impact of converter parameters is analyzed, which provides a guideline for converter parameter settings design.

Appendix

The model parameters settings are listed in Table I.

TABLE I: Parameters Settings

Parameters	Description	Value
E_g	Grid voltage	230 Vrms
ω_n	Grid frequency	100π rad/s
P_{setSG}	SG nominal power	30kW
P_{setCON}	Converter nominal active power	3kW
S_{nCON}	Converter nominal apparent power	3kVA
ΔP_L	Load step	3kW
SCR	Short Circuit Ratio	30
T_g	Governor time constant	0.2s
T_{rh}	Re-heater turbine time constant	7s
ω_f	Low pass filter bandwidth	100π rad/s
D_p	Damping coefficient	45 Ws/rad

Acknowledgment

ECS4DRES is supported by the Chips Joint Undertaking under grant agreement number 101139790 and its members, including the top-up funding by Germany, Italy, Slovakia, Spain and The Netherlands.

References

[1] N. Hatziargyriou, J. Milanovic, C. Rahmann, V. Ajjarapu, C. Canizares, I. Erlich, D. Hill, I. Hiskens, I. Kamwa, B. Pal, P. Pourbeik, J. Sanchez-Gasca, A. Stankovic, T. Van Cutsem, V. Vittal, and C. Vournas, "Definition and classification of power system stability – revisited extended," *IEEE Transactions on Power Systems*, vol. 36, no. 4, pp. 3271–3281, 2021.

[2] J. Xiao, L. Wang, P. Bauer, and Z. Qin, "A consensus algorithm-based secondary control with low vulnerability in microgrids," *IEEE Transactions on Industrial Informatics*, pp. 1–10, 2025.

[3] J. Xiao, L. Wang, Y. Wan, P. Bauer, and Z. Qin, "Distributed model predictive control-based secondary control for power regulation in ac microgrids," *IEEE Transactions on Smart Grid*, vol. 15, no. 6, pp. 5298–5308, 2024.

[4] J. Xiao, L. Wang, Z. Qin, and P. Bauer, "A resilience enhanced secondary control for ac micro-grids," *IEEE Transactions on Smart Grid*, vol. 15, no. 1, pp. 810–820, 2024.

[5] B. Tan, J. Zhao, M. Netto, V. Krishnan, V. Terzija, and Y. Zhang, "Power system inertia estimation: Review of methods and the impacts of converter-interfaced generations," *International Journal of Electrical Power Energy Systems*, vol. 134, 07 2021.

[6] J. Matevosyan, B. Badrzadeh, T. Prevost, E. Quitmann, D. Ramasubramanian, H. Urdal, S. Achilles, J. MacDowell, S. H. Huang, V. Vital, J. O'Sullivan, and R. Quint, "Grid-forming inverters: Are they the key for high renewable penetration?" *IEEE Power and Energy Magazine*, vol. 17, no. 6, pp. 89–98, 2019.

[7] A. Tayyebi, D. Groß, A. Anta, F. Kupzog, and F. Dörfler, "Frequency stability of synchronous machines and grid-forming power converters," *IEEE Journal of Emerging and Selected Topics in Power Electronics*, vol. 8, no. 2, pp. 1004–1018, 2020.

[8] B. Tan, J. Zhao, M. Netto, V. Krishnan, V. Terzija, and Y. Zhang, "Power system inertia estimation: Review of methods and the impacts of converter-interfaced generations," *International Journal of Electrical Power Energy Systems*, vol. 134, p. 107362, 2022. [Online]. Available: https://www.sciencedirect.com/science/article/pii/S0142061521006013

[9] Y. Qi, H. Deng, X. Liu, and Y. Tang, "Synthetic inertia control of grid-connected inverter considering the synchronization dynamics," *IEEE Transactions on Power Electronics*, vol. 37, no. 2, pp. 1411–1421, 2022.

[10] J. Van de Vyver, J. D. M. De Kooning, B. Meersman, L. Vandevelde, and T. L. Vandoorn, "Droop control as an alternative inertial response strategy for the synthetic inertia on wind turbines," *IEEE Transactions on Power Systems*, vol. 31, no. 2, pp. 1129–1138, 2016.

[11] S.-K. Chung, "A phase tracking system for three phase utility interface inverters," *IEEE Transactions on Power Electronics*, vol. 15, no. 3, pp. 431–438, 2000.

[12] L. Zhang, L. Harnefors, and H.-P. Nee, "Power-synchronization control of grid-connected voltage-source converters," *IEEE Transactions on Power Systems*, vol. 25, no. 2, pp. 809–820, 2010.

[13] K. De Brabandere, B. Bolsens, J. Van den Keybus, A. Woyte, J. Driesen, and R. Belmans, "A voltage and frequency droop control method for parallel inverters," *IEEE Transactions on Power Electronics*, vol. 22, no. 4, pp. 1107–1115, 2007.

[14] S. You, H. Li, S. Liu, K. Sun, W. Wang, W. Qiu, and Y. Liu, "Calculate center-of-inertia frequency and system rocof using pmu data," in *2021 IEEE Power Energy Society General Meeting (PESGM)*, 2021, pp. 1–5.

[15] E. Ducoin, Y. Gu, B. Chaudhuri, and T. Green, "Swing equation modelling of gfl inverter and comparison of its damping and inertia with gfm inverter," vol. 2023, 03 2023, pp. 108–114.